Fitness seascapes promote genetic heterogeneity through spatiotemporally distinct mutant selection windows

Eshan S. King[1], Beck Pierce[2], Michael Hinczewski[3], and Jacob G. Scott[1,3,4,*]

[1]Systems Biology and Bioinformatics Program, School of Medicine, Case Western Reserve University, Cleveland, OH, USA
[2]Department of Mathematics, Applied Mathematics, and Statistics, Case Western Reserve University, Cleveland, OH
[3]Department of Physics, Case Western Reserve University, Cleveland, OH, USA
[4]Department of Translational Hematology and Oncology Research, Cleveland Clinic, Cleveland, OH, USA
[*]scottj10@ccf.org

ABSTRACT

Mutant selection windows (MSWs), the range of drug concentrations that select for drug-resistant mutants, have long been used as a model for predicting drug resistance and designing optimal dosing strategies in infectious disease. The canonical MSW model only offers comparisons between two phenotypes at a time: sensitive and resistant. The fitness landscape model with N alleles allows comparisons between N genotypes simultaneously, but does not encode drug dosing data. In clinical settings, there may be a wide, spatio-temporal range of drug concentrations selecting for a variety of adaptive genotypes. There is a need for a more robust model of the pathogen response to therapy to predict resistance and design optimal dosing strategies. Fitness seascapes, which model genotype-by-environment interactions, permit multiple MSW comparisons simultaneously by encoding genotype-specific dose-response data. In this work, we show how N-allele fitness seascapes embed $N * 2^N$ unique MSW comparisons. In three clinically relevant pharmacokinetic models, we show how fitness seascapes reveal heterogeneous MSWs, extending the MSW model to more accurately reflect the selection of drug resistant genotypes. Our work highlights the importance and utility of considering dose-dependent fitness seascapes in evolutionary medicine.

Introduction

Predicting the molecular evolution of drug resistance in infectious disease may allow us to design adaptive therapies to avoid resistance or leverage known drug resistance mechanisms to make rational therapy decisions. The concept of the mutant selection window (MSW), the range of drug concentrations where the mutant growth rate is not fully suppressed and is higher than the wild-type, has been studied as a means of predicting evolution and optimizing drug regimens[1–9]. Under the MSW paradigm, drug regimens should be chosen that minimize time spent with drug concentration in the MSW[9,10]. Previous work with MSWs has shown how patient nonadherence and tissue compartmentalization confounds this principle, allowing for the emergence of drug resistant mutants[6,8,11,12].

MSWs only offer comparisons between two genotypes or phenotypes at a time– i.e., between the drug susceptible reference genotype and the drug resistant genotype. In comparison, fitness landscapes, which are mappings from genotype to fitness, offer comparisons of many genotypes simultaneously. For instance, in the binary landscape model with N mutational sites, each genotype may be simultaneously compared to N adjacent genotypes[13–20].

Fitness seascapes extend the fitness landscape model by mapping both genotype and environment (i.e. drug concentration) to fitness[7,19,21–24]. In this work, we map genotypes to random drug dose-response curves to simulate fitness seascapes. Das et al. have previously shown that MSWs are intrinsically embedded in fitness seascapes[7]. Here, we expand on this idea and explore the MSW model through the lens of fitness seascapes. First, we show how an N-allele fitness seascape embeds $N * 2^N$ unique MSW comparisons. Then, we model drug concentration variation in time and space in three clinically-relevant scenarios, revealing the presence of heterogeneous MSWs. While other work has analyzed the importance of time spent in a MSW, we also consider the impact of the amount of space occupied by a MSW. We argue that both time and space occupied by a MSW may impact the probability of resistance.

This work further explores the connection between MSWs and fitness seascapes using realistic pharmacokinetic and drug diffusion models. Our results highlight the importance of fitness seascapes in modeling evolution when drug concentration varies in time and space. Furthermore, because of the multiplicity of MSWs present in a fitness seascape, this work suggests

that a higher-dimensional MSW model offered by fitness seascapes may be more powerful for predicting evolution.

Results and Discussion

Fitness seascapes embed mutant selection window data

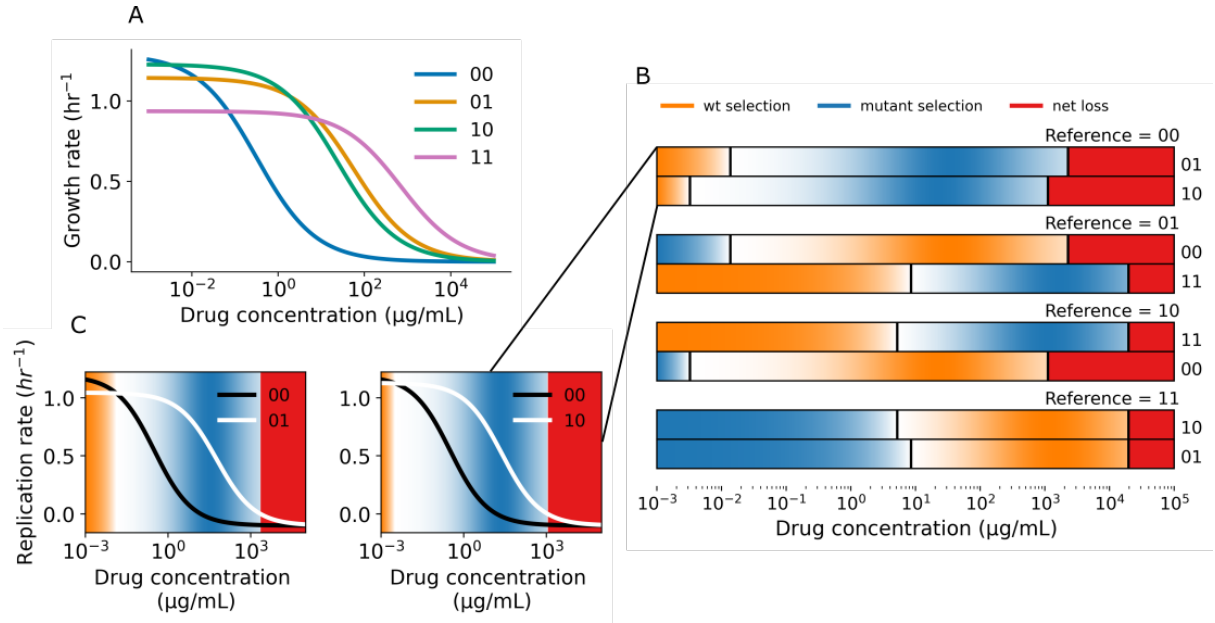

Figure 1. **Fitness seascapes embed MSW data.** **A**) Simulated 2-allele fitness seascape used to generate this MSW data. **B**) All 8 ($8 = N * 2^N, N = 2$) MSW comparisons for a 2-allele fitness seascape. Each two row group represents a single reference genotype compared to its two neighboring genotypes. Wild-type selection, mutant selection, and net loss windows are calculated as a function of drug concentration and shown as colored rectangles. Wild-type selection windows and MSWs are also shaded by the normalized selection coefficient. **C**) Example MSWs shown over the corresponding dose-response curves. The black line (00) is the dose-response curve for the reference genotype, while the white lines are considered the mutant genotypes.

We first investigated how multiple MSWs are embedded in fitness seascapes. Here, we model genotypes as binary strings of length N, with a zero indicating no mutation and a 1 indicating a mutation in a given position. N represents the total number of resistance-conferring mutations considered. These mutations can be thought of as either single nucleotide polymorphisms, single amino acid substitutions, or larger chromosomal changes. We model a simple 2-allele fitness seascape by mapping a combinatorially complete set of genotypes (00, 01, 10, 11) to random dose-response curves (**Fig. 1A**). Dose response curves differ in their IC_{50} and drug-free growth rates. Empirical fitness seascapes bearing a similar structure and demonstrating fitness tradeoffs have been reported by others[7,19,25].

In an N-allele model, each genotype can be compared to N neighboring genotypes. Thus, given that each genotype can be thought of as the 'reference genotype', an N-allele fitness seascape embeds $N * 2^N$ MSW comparisons. If one includes only *unique* MSW comparisons, i.e. the distinction between reference and comparison genotype is not meaningful, then this expression is $N * 2^N/2$. This connection is illustrated in **Fig. 1B**, where the grid of all possible MSWs is shown for a 2-allele seascape. The MSWs and wild-type selection windows are also shaded by the relative selection coefficient, $s_{i,j}$, which is defined as the normalized ratio between the growth rates under comparison:

$$s_{i,j} = \frac{g_i}{g_j}, \tag{1}$$

where g_i represents the growth rate of the genotype under selection and g_j represents the growth rate of the less fit genotype. An example comparison with dose-response curves is shown in **Fig. 1C**. Notably, the strength of selection blurs between the boundaries of the selection windows, further complicating the MSW paradigm (**Fig. 1B**). It may be useful to consider where selection is strongest within a MSW when designing dosing strategies.

Multiple mutant selection windows arise when drug concentration varies in time and space

We next sought to investigate MSWs in physiologically-relevant temporal and spatial models of drug kinetics. First, to illustrate MSWs in time, we simulated a patient undergoing a daily drug dosing regimen with a constant rate of nonadherence, using

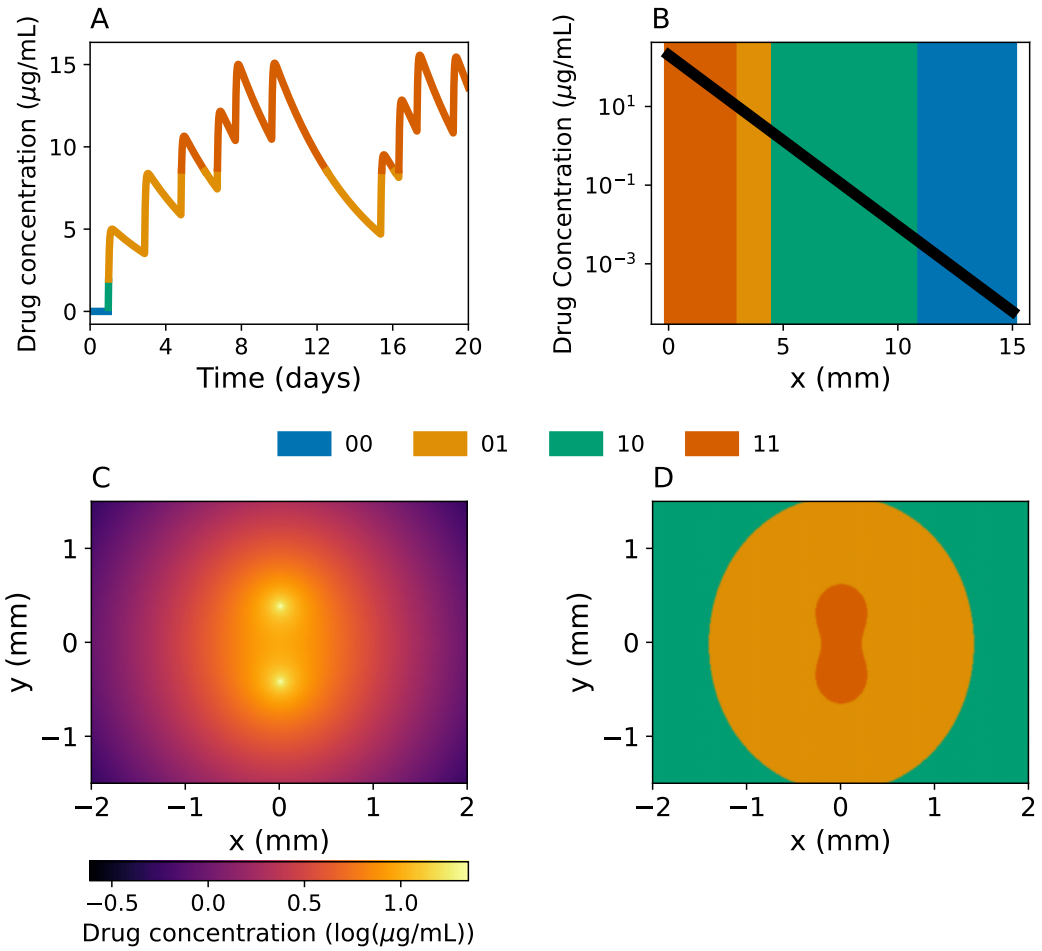

Figure 2. 1- and 2-D pharmacokinetic models reveal diverse MSWs. A) Drug concentration in time in a simulated patient undergoing a daily oral antibiotic regimen with a high level of nonadherence. Colors in the trace represent the mutant under selection at a given drug concentration. **B)** Simulated 1-D drug diffusion in tissue from a blood vessel placed at x = 0. The black line represents the drug concentration, while the color represents the MSW at that region. **C)** Resulting 2-D steady state drug diffusion from two blood vessels placed at (0, -0.4) and (0, 0.4). **D)** Spatial MSWs corresponding to **C**. All fitness data is based on the seascape in Fig. 1.

methods described by King et al[25]. Briefly, we model the serum drug concentration using a 1-compartment pharmacokinetic model and convolve this model with an impulse train with each impulse representing a correctly administered drug dose (see Methods). We found that patient serum drug concentrations can fluctuate in and out of MSWs depending on the individual patient's nonadherence pattern. A representative drug concentration trace is shown in **Fig. 2 A** where the drug concentration trace is colored by the current selection window. In this patient, the drug concentration quickly builds to over 10 μg/mL, reaching the double mutant selection window. However, the patient misses several days of drug doses in a row, and the serum concentration drops back into the 01 genotype selection window. Fluctuating selection windows may be minimized with stricter adherence or strategies that quickly achieve steady-state, such as a loading dose.

Another important pharmacokinetic consideration is drug diffusion in tissue. We use a partial differential equation (Eq. 2) to find a steady state solution of drug diffusion from a blood vessel in 1 spatial dimension (1-D):

$$\frac{\partial}{\partial t}u(x,t) = D\frac{\partial^2}{\partial x^2}u(x,t) - \gamma u(x,t) + k\delta(x). \tag{2}$$

The 1D steady-state solution is of the form:

$$u(x) = \frac{k}{\sqrt{4D\gamma}}\exp\left(-|x|\sqrt{\frac{\gamma}{D}}\right). \tag{3}$$

Here, D represents a drug-dependent diffusion constant; γ is a rate at which the drug is metabolized, consumed, or cleared; and k represents the drug concentration at the tissue-blood vessel boundary. We model a blood vessel source at $x = 0$ and compute drug concentration as a function of distance from the blood vessel. Using a similar approach to before, we used information embedded in the fitness seascape to identify MSWs in space. Drug diffusion results in four different MSWs across the simulated tissue (**Fig. 2B**). These results demonstrate that, given a constant concentration of a drug source in a tissue compartment, multiple mutatnt selection windows may exist simultaneously.

To better understand spatial heterogeneity, we modeled drug diffusion in 2 dimensions (2D) with a similar partial differential equation as before (see methods). The steady-state drug concentration is given by:

$$u(r) = \frac{k}{2\pi D}K_0\left(\sqrt{\frac{\gamma}{D}}r\right), \tag{4}$$

where $K_0(\cdot)$ is a modified Bessel function of the second kind and r is the radial distance from the blood vessel source. We then considered the spatial effects of multiple blood vessels in two dimensions, allowing for a more sophisticated representation of MSWs in tissue. The distinction between 1 and 2 spatial dimensions is important, as the space occupied by a MSW in 2D scales by the distance from the blood vessel squared. The steady-state drug concentration profile is shown in **Fig. 2C**, with two blood vessels placed at (0,-0.4) and (0,0.4). Applying the MSW mask reveals 3 distinct windows in this regime (**Fig. 2D**), with the 11 window appearing to 'bridge' the two blood vessels.

This 2D model offers a more complete picture of the MSWs functionally existing in an area around two blood vessels. These results suggest that including drug diffusion and pharmacodynamic effects may be important for simulating and predicting evolution with spatial considerations. Introducing more blood vessels with arbitrary patterns would further complicate the drug diffusion pattern and the resulting MSWs. Together, these results complicate the singular notion of a MSW describing the evolution of drug resistance. Instead, multiple MSWs may dictate evolution within a single population across time and space.

Conclusions

In this work, we have shown how rich MSW data is embedded in fitness seascapes and how numerous MSWs may exist when the selection pressure, in this case drug concentration, varies in time and space. Notably, by simulating the serum drug concentration in a patient with moderate nonadherence, we have shown how the drug concentration may oscillate between MSWs. Furthermore, in a simple model of drug diffusion from a blood vessel, we have shown how multiple MSWs may exist simultaneously in space. These results suggest that fitness seascapes may expand the power of MSW models to predict evolution when drug concentration varies in time and space.

Others have shown computationally and experimentally that drug diffusion gradients and differential drug penetration, which permit heterogeneous MSWs, facilitate antibiotic resistance[11,]. Considering drug pharmacokinetics in time, Nande and Hill, among others, have shown that drug absorption rate and patient nonadherence can impact the evolution of resistance[12,25]. Our results suggest that this is likely a function of both the time spent in the MSW and, in the case of nonadherence, the drug concentration dropping back down into a MSW.

Incorporating PK/PD models and MSWs may be crucial for predicting evolution in the clinic; indeed, Pan et al have demonstrated the presence of an MSW for *Pseudomonas aeruginosa* in an *in vivo* model, showing a correlation between

suboptimal PK/PD parameters and the emergence of drug resistance[27]. In addition, random spatial blood vessel arrangements may confer additional heterogeneity[28]. In the future, we may leverage fitness seascape data and the MSW analysis framework to more accurately predict the evolution of drug resistance. In addition, a simple geometric model of overlapping MSWs may reveal alternative paths to specific genotypes. This may permit the 'driving' of evolving populations to specific genetic states, allowing us to exploit known mechanisms of resistance[29]. For instance, we may use this approach to leverage collateral sensitivity, where evolved resistance to one drug confers sensitivity to another[30,31].

Methods

Serum drug concentration over time with nonadherence

Patient serum concentrations, $c(t)$, are modeled with a 1-compartment pharmacokinetic model:

$$c(t) = c_{max}[e^{-k_{elim}t} - e^{-k_{abs}t}], \tag{5}$$

where k_{abs} and k_{elim} represent absorption and elimination rates and c_{max} represents the maximum drug concentration. Drug doses are simulated with an impulse train, with each impulse representing a dose. Serum concentration over time for each patient is computed by convolving the drug dose impulse train with the pharmacokinetic model. Formally, this is done by generating a set (D) of numbers representing the time of each scheduled drug dose. Then, for each patient, a random subset of drug doses are removed from D, with each drug dose having a constant probability p_{forget} of being removed, resulting in the set of drug doses that the simulated patient correctly self administered (D_a). A Dirac comb is generated using D_a with the period T equal to the time between drug doses (Eq. 6):

$$III_a(t) = \sum_{d \in D_a} \delta(t - dT), \tag{6}$$

and the resulting impulse train is convolved with the pharmacokinetic model in Eq. 5 to generate the simulated patient's serum drug concentration (Eq. 7):

$$c_{patient}(t) = c(t) \circledast III_a(t). \tag{7}$$

Diffusion with a delta source and constant absorption

We modeled the drug concentration gradient that a population may experience as a point source with diffusion and constant absorption. The point source represents drug diffusion from a blood vessel, while constant absorption encapsulates clearance, metabolism, and consumption of drug. Formally, we want to track the concentration on an infinite domain, with diffusion described by diffusivity D, absorption at every position described by a rate $\gamma > 0$, and a source term that is a Kronecker delta with strength $k > 0$ at the origin $x = 0$. The diffusion equation then takes the form:

$$\frac{\partial}{\partial t}u(x,t) = D\frac{\partial^2}{\partial x^2}u(x,t) - \gamma u(x,t) + k\delta(x). \tag{8}$$

We assume we initially have zero concentration everywhere, so $u(x,0) = 0$. To solve this, we will Fourier transform the above equation:

$$u(x,t) = \frac{1}{2\pi}\int_{-\infty}^{\infty} dy\, e^{ixy}\tilde{u}(y,t), \tag{9}$$

where $\tilde{u}(y,t)$ is the Fourier transform of $u(x,t)$. Now let us take time and space derivatives of Eq. (9), which we will later substitute into Eq. (8):

$$\begin{aligned}
\frac{\partial}{\partial t}u(x,t) &= \frac{1}{2\pi}\int_{-\infty}^{\infty} dy\, e^{ixy}\frac{\partial}{\partial t}\tilde{u}(y,t),\\
\frac{\partial}{\partial x}u(x,t) &= \frac{1}{2\pi}\int_{-\infty}^{\infty} dy\, iye^{ixy}\tilde{u}(y,t),\\
\frac{\partial^2}{\partial x^2}u(x,t) &= \frac{1}{2\pi}\int_{-\infty}^{\infty} dy\,(-y^2)e^{ixy}\tilde{u}(y,t).
\end{aligned} \tag{10}$$

The final fact that we need is the Fourier transform of the Dirac delta function,

$$\delta(x) = \frac{1}{2\pi}\int_{-\infty}^{\infty} dy\, e^{ixy}. \tag{11}$$

Substituting Eqs. (9)-(11) into Eq. (8), and collecting everything on one side under the same integral, we get:

$$\frac{1}{2\pi}\int_{-\infty}^{\infty} dy\, e^{ixy}\left(\frac{\partial}{\partial t}\tilde{u}(y,t)+Dy^2\tilde{u}(y,t)+\gamma\tilde{u}(y,t)-k\right)=0. \tag{12}$$

In order for Eq. (12) to be true for any x, the terms in the parentheses have to equal to zero. This yields an ordinary, first-order differential equation for $\tilde{u}(y,t)$:

$$\frac{\partial}{\partial t}\tilde{u}(y,t)=-(Dy^2+\gamma)\tilde{u}(y,t)+k. \tag{13}$$

Using the initial condition $u(x,0)=0$, we find the solution for $\tilde{u}(y,t)$:

$$\tilde{u}(y,t)=\frac{-k}{Dy^2+\gamma}\left(e^{-t(Dy^2+\gamma)}-1\right). \tag{14}$$

Substituting into Eq. (9) and rearranging we get our final answer for $u(x,t)$:

$$u(x,t)=\frac{1}{2\pi}\int_{-\infty}^{\infty} dy\,\frac{e^{ixy}\left(1-e^{-t\left(Dy^2+\gamma\right)}\right)k}{Dy^2+\gamma}. \tag{15}$$

In the limit $t\to\infty$ the concentration profile approaches a stationary distribution that is analytically solvable (since the integral can be carried out when $t\to\infty$):

$$u(x,\infty)=\frac{k}{\sqrt{4D\gamma}}\exp\left(-|x|\sqrt{\frac{r}{D}}\right). \tag{16}$$

Diffusion with a delta source and constant absorption in two dimensions

Wishing to model a similar drug concentration space based on blood vessel origin points, we instead look at the diffusion modeled in two-dimensional space using polar coordinates. We begin with the same modeling technique as Eq. (8) but in two dimensions:

$$\frac{\partial}{\partial t}u(x_1,x_2,t)=D\left[\frac{\partial^2}{\partial x_1^2}+\frac{\partial^2}{\partial x_2^2}\right]u(x_1,x_2,t)-\gamma u(x_1,x_2,t)+k\delta^{(2)}(x_1,x_2). \tag{17}$$

Here $\delta^{(2)}(x_1,x_2)$ is the 2D Dirac delta, $\delta^{(2)}(x_1,x_2)=\delta(x_1)\delta(x_2)$ which represents our source. We know by symmetry that the solution will only depend on the radial coordinate, $u(x_1,x_2,t)=u(r,t)$, where $r=\sqrt{x_1^2+x_2^2}$. However it is easier to proceed with the Fourier transform first in Cartesian coordinates, so we will delay the transformation to polar coordinates until later. The 2D Fourier transform is:

$$u(x_1,x_2,t)=\frac{1}{(2\pi)^2}\int_{-\infty}^{\infty} dy_1dy_2\, e^{i(x_1y_1+x_2y_2)}\tilde{u}(y_1,y_2,t). \tag{18}$$

We calculate the time and space derivatives analogously to Eqs. (10)-(11), and the result is the 2D version of Eq. (12):

$$\frac{1}{(2\pi)^2}\int_{-\infty}^{\infty} dy_1dy_2\, e^{i(x_1y_1+x_2y_2)}\left(\frac{\partial}{\partial t}\tilde{u}(y_1,y_2,t)+D(y_1^2+y_2^2)\tilde{u}(y_1,y_2,t)+\gamma\tilde{u}(y_1,y_2,t)-k\right)=0. \tag{19}$$

Converting to polar coordinates for both the original and Fourier variables: $x_1=r\cos\theta$, $x_2=r\sin\theta$, $y_1=\rho\cos\psi$, $y_2=\rho\sin\psi$. By symmetry we know that $\tilde{u}(y_1,y_2,t)=\tilde{u}(\rho,t)$, where $\rho=\sqrt{y_1^2+y_2^2}$. Eq. (19) becomes:

$$\frac{1}{(2\pi)^2}\int_0^{\infty} d\rho\int_0^{2\pi} d\psi\rho\, e^{ir\rho\cos(\psi-\theta)}\left(\frac{\partial}{\partial t}\tilde{u}(\rho,t)+D\rho^2\tilde{u}(\rho,t)+\gamma\tilde{u}(\rho,t)-k\right)=0. \tag{20}$$

For this equation to be always true, the terms in the parentheses must be zero, giving:

$$\frac{\partial}{\partial t}\tilde{u}(\rho,t)=-(D\rho^2+\gamma)\tilde{u}(y,t)+k. \tag{21}$$

This has exactly the same form as Eq. (13), and hence the solution looks like Eq. (14):

$$\tilde{u}(\rho,t) = \frac{-k}{D\rho^2+\gamma}\left(e^{-t(D\rho^2+\gamma)}-1\right). \tag{22}$$

The real space solution $u(x_1,x_2,t) = u(r,\theta,t)$ in polar coordinates is just the inverse Fourier transform of the above:

$$\begin{aligned} u(r,\theta,t) &= \frac{1}{(2\pi)^2}\int_0^\infty d\rho \int_0^{2\pi} d\psi \rho\, e^{ir\rho\cos(\psi-\theta)} \frac{k}{D\rho^2+\gamma}\left(1-e^{-t(D\rho^2+\gamma)}\right) \\ &= \frac{1}{2\pi}\int_0^\infty d\rho \frac{k\rho J_0(r\rho)}{D\rho^2+\gamma}\left(1-e^{-t(D\rho^2+\gamma)}\right). \end{aligned} \tag{23}$$

Here $J_0(z)$ is a Bessel function of the first kind. Note that the θ dependence has been integrated out, so $u(r,\theta,t) = u(r,t)$, as expected by symmetry. As before, this integral cannot be carried out analytically, but can be easily approximated numerically. To find the steady-state solution, we take the $t \to \infty$ limit, in which case the integral above evaluates to:

$$\begin{aligned} u(r,t=\infty) &= \frac{1}{2\pi}\int_0^\infty d\rho \frac{k\rho J_0(r\rho)}{D\rho^2+\gamma} \\ &= \frac{k}{2\pi D} K_0\left(\sqrt{\frac{\gamma}{D}}r\right). \end{aligned} \tag{24}$$

Here $K_0(z)$ is a modified Bessel function of the second kind. This function diverges at zero, which proves problematic for calculating concentrations near the proposed vessels. Instead, we choose a blood vessel radius and set the drug concentration within that radius equal to a constant maximum drug concentration. Thus, this analysis holds more strongly for analysis away from the immediate vicinity of the vessel.

To model drug diffusion from an arbitrary number of sources, we convolved the discretized version of Eq. (24) ($u_{i,j}(t=\infty)$) with a 2D matrix of point sources ($\Delta_{i,j}$), where (i,j) represents position in the discretized space:

$$U_{i,j} = u_{i,j}(t=\infty) \circledast \Delta_{i,j}. \tag{25}$$

References

1. Drlica, K. The mutant selection window and antimicrobial resistance. *J. Antimicrob. Chemother.* **52**, 11–17, DOI: 10.1093/jac/dkg269 (2003).
2. Firsov, A. A. *et al.* In vitro pharmacodynamic evaluation of the mutant selection window hypothesis using four fluoroquinolones against staphylococcus aureus. *Antimicrob. Agents Chemother.* **47**, 1604–1613, DOI: 10.1128/AAC.47.5.1604-1613.2003 (2003).
3. Blondeau, J., Hansen, G., Metzler, K. & Hedlin, P. The role of pk/pd parameters to avoid selection and increase of resistance: Mutant prevention concentration. *J. Chemother.* **16**, 1–19, DOI: 10.1080/1120009X.2004.11782371 (2004).
4. Drlica, K. & Zhao, X. Mutant selection window hypothesis updated. *Clin. Infect. Dis.* **44**, 681–688, DOI: 10.1086/511642 (2007).
5. Olofsson, S. K. & Cars, O. Optimizing drug exposure to minimize selection of antibiotic resistance. *Clin. Infect. Dis.* **45**, S129–S136, DOI: 10.1086/519256 (2007).
6. Rosenbloom, D. I. S., Hill, A. L., Rabi, S. A., Siliciano, R. F. & Nowak, M. A. Antiretroviral dynamics determines hiv evolution and predicts therapy outcome. *Nat. Medicine* **18**, 1378–1385, DOI: 10.1038/nm.2892 (2012).
7. Das, S. G., Direito, S. O., Waclaw, B., Allen, R. J. & Krug, J. Predictable properties of fitness landscapes induced by adaptational tradeoffs. *eLife* **9**, e55155, DOI: 10.7554/eLife.55155 (2020).
8. Feder, A. F., Harper, K. N., Brumme, C. J. & Pennings, P. S. Understanding patterns of hiv multi-drug resistance through models of temporal and spatial drug heterogeneity. *eLife* **10**, e69032, DOI: 10.7554/eLife.69032 (2021).
9. Firsov, A. A., Portnoy, Y. A., Strukova, E. N., Shlykova, D. S. & Zinner, S. H. Predicting bacterial resistance using the time inside the mutant selection window: Possibilities and limitations. *Int. J. Antimicrob. Agents* **44**, 301–305, DOI: 10.1016/j.ijantimicag.2014.06.013 (2014).

10. Alieva, K. N. *et al.* Time inside the mutant selection window as a predictor of staphylococcal resistance to linezolid. *The J. Antibiot.* **71**, 514–521, DOI: 10.1038/s41429-017-0016-9 (2018).

11. Moreno-Gamez, S. *et al.* Imperfect drug penetration leads to spatial monotherapy and rapid evolution of multidrug resistance. *Proc. Natl. Acad. Sci.* **112**, E2874–E2883, DOI: 10.1073/pnas.1424184112 (2015).

12. Nande, A. & Hill, A. L. The risk of drug resistance during long-acting antimicrobial therapy. *Proc. Royal Soc. B: Biol. Sci.* **289**, 20221444, DOI: 10.1098/rspb.2022.1444 (2022).

13. Gillespie, J. H. A simple stochastic gene substitution model. *Theor. Popul. Biol.* **23**, 202–215, DOI: 10.1016/0040-5809(83)90014-X (1983).

14. Gillespie, J. H. Some properties of finite populations experiencing strong selection and weak mutation. *The Am. Nat.* **121**, 691–708, DOI: 10.1086/284095 (1983).

15. Gillespie, J. H. Molecular evolution over the mutational landscape. *Evolution* **38**, 1116, DOI: 10.2307/2408444 (1984).

16. Weinreich, D. M., Delaney, N. F., DePristo, M. A. & Hartl, D. L. Darwinian evolution can follow only very few mutational paths to fitter proteins. *Science* **312**, 111–114, DOI: 10.1126/science.1123539 (2006).

17. Kouyos, R. D. *et al.* Exploring the complexity of the hiv-1 fitness landscape. *PLoS Genet.* **8**, e1002551, DOI: 10.1371/journal.pgen.1002551 (2012).

18. Mira, P. M. *et al.* Rational design of antibiotic treatment plans: A treatment strategy for managing evolution and reversing resistance. *PLOS ONE* **10**, e0122283, DOI: 10.1371/journal.pone.0122283 (2015).

19. Ogbunugafor, C. B., Wylie, C. S., Diakite, I., Weinreich, D. M. & Hartl, D. L. Adaptive landscape by environment interactions dictate evolutionary dynamics in models of drug resistance. *PLOS Comput. Biol.* **12**, e1004710, DOI: 10.1371/journal.pcbi.1004710 (2016).

20. Maltas, J., McNally, D. M. & Wood, K. B. Evolution in alternating environments with tunable interlandscape correlations. *Evolution* **75**, 10–24, DOI: 10.1111/evo.14121 (2021).

21. Merrell, D. J. *The Adaptive Seascape: The Mechanism of Evolution* (University of Minnesota Press, 1994), minne ed. edition edn.

22. Lässig, M., Mustonen, V. & Walczak, A. M. Predicting evolution. *Nat. Ecol. & Evol.* **1**, 0077, DOI: 10.1038/s41559-017-0077 (2017).

23. Mustonen, V. & Lässig, M. From fitness landscapes to seascapes: non-equilibrium dynamics of selection and adaptation. *Trends Genet.* **25**, 111–119, DOI: 10.1016/j.tig.2009.01.002 (2009).

24. Agarwala, A. & Fisher, D. S. Adaptive walks on high-dimensional fitness landscapes and seascapes with distance-dependent statistics. *Theor. Popul. Biol.* **130**, 13–49, DOI: 10.1016/j.tpb.2019.09.011 (2019).

25. King, E. S. *et al.* Fitness seascapes are necessary for realistic modeling of the evolutionary response to drug therapy. *biorxiv* DOI: 10.1101/2022.06.10.495696 (2022).

26. Fuentes-Hernández, A., Hernández-Koutoucheva, A., Muñoz, A. F., Domínguez Palestino, R. & Peña-Miller, R. Diffusion-driven enhancement of the antibiotic resistance selection window. *J. The Royal Soc. Interface* **16**, 20190363, DOI: 10.1098/rsif.2019.0363 (2019).

27. Pan, A.-j. *et al.* Validation of the mutant selection window hypothesis with fosfomycin against escherichia coli and pseudomonas aeruginosa: an in vitro and in vivo comparative study. *The J. Antibiot.* **70**, 166–173, DOI: 10.1038/ja.2016.124 (2017).

28. Scott, J. G., Fletcher, A. G., Anderson, A. R. A. & Maini, P. K. Spatial metrics of tumour vascular organisation predict radiation efficacy in a computational model. *PLOS Comput. Biol.* **12**, e1004712, DOI: 10.1371/journal.pcbi.1004712 (2016).

29. Nichol, D. *et al.* Steering evolution with sequential therapy to prevent the emergence of bacterial antibiotic resistance. *PLOS Comput. Biol.* **11**, e1004493, DOI: 10.1371/journal.pcbi.1004493 (2015).

30. Nichol, D. *et al.* Antibiotic collateral sensitivity is contingent on the repeatability of evolution. *Nat. Commun.* **10**, 334, DOI: 10.1038/s41467-018-08098-6 (2019).

31. Iram, S. *et al.* Controlling the speed and trajectory of evolution with counterdiabatic driving. *Nat. Phys.* **17**, 135–142, DOI: 10.1038/s41567-020-0989-3 (2021).